Two-dimensional structures of electron bunches in relativistic plasma cavities

Lars Reichwein,* Johannes Thomas, and Alexander Pukhov

Institut für Theoretische Physik I, Heinrich-Heine-Universität Düsseldorf, D-40225 Düsseldorf, Germany

The spatial structure of an ultralow-emittance electron bunch in a plasma wakefield blowout regime is studied. The full Liénard-Wiechert potentials are considered for mutual interparticle interactions in the framework of the equilibrium slice model. This model uses the quasistatic theory which allows one to solve the Liénard-Wiechert potentials without knowledge of the electrons' history. The equilibrium structure we find is similar to already observed hexagonal lattices but shows topological defects. Scaling laws for interparticle distances are obtained from numerical simulations and analytical estimations.

I. INTRODUCTION

Plasma-based electron acceleration methods are known for their high efficiency, which allows one to accelerate electrons up to some GeV over much shorter distances than in conventional accelerators [1]. In the field of laser-driven plasma acceleration, the wakefield is excited by an intense laser pulse with wavelength λ_L, duration τ, and focal spot size R [2,3]. In plasmas with homogeneous density, the wakefield breaks as soon as the laser pulse intensity reaches a certain threshold value and the normalized laser amplitude $a_0 > 1$. If $a_0 > 4$ and $R > 2\lambda_L$ and if the laser pulse perfectly fits into the first half of the plasma period, a solitary electronic cavity, called the bubble, is formed [4–7]. It is a nearly spherical region with uniform accelerating fields that propagates with almost speed of light c [8] and traps background electrons at its tail. The major features that characterize the bubble regime are the quasimonoenergetic spectrum of the fast electrons and a quasistatic laser pulse, which propagates many Rayleigh lengths in homogeneous plasma without significant diffraction. Another method to excite a plasma wakefield is to use a charged particle beam with length σ_z, radius σ_r, and density n_b [9,10]. If the particle beam is thin, $\sigma_z \approx \sqrt{2}k_p^{-1} \gg \sigma_r$, and if its density much larger than the electron plasma density, a structure similar to the bubble, the so-called blow-out, is created. In both cases, a nearly harmonic wakefield potential accelerates trapped electrons to high energies and focuses them to the axis where they form a dense electron beam—the so-called beam load.

Two promising methods to control the beam-load formation are the density down-ramp and the ionization injection technique. Both methods produce witness electron beams with sub-fs temporal duration, a very high peak current of several kA, energy spreads well below 1%, and an excellent transverse emittance [11–16]. The density down-ramp injection is reached by a longitudinal modulation of the plasma density with potentially extremely large gradients (also known as shock fronts) [17–20]. The ionization injection requires a small

amount of higher-Z gas, added to the gas used for acceleration [21,22]. If the wakefield is driven by a short electron beam, the Trojan horse regime of underdense photocathode plasma wakefield acceleration is reached [23,24]. It is best suited to decouple the electron bunch generation process from the excitation of the accelerating plasma cavity. The combination of the nonrelativistic intensities required for tunnel ionization (10^{14} W/cm^2), a localized release volume as small as the laser focus, the greatly minimized transverse momenta, and the rapid acceleration leads to dense phase-space packets. In homogeneous plasma they can have ultralow normalized transverse emittance in the bulk of μm mrad and a minimal energy spread in the 0.1% range [23,25].

In addition to the aim to produce electron bunches with highest energies and smallest transverse emittances, it is also important to discuss the spatial beam-load structure. In some recent experiments the length, the diameter, and the emittance of the beam load were measured to determine the beam quality [26,27]. If, however, the relativistic emittance falls below a certain threshold value and if the electron energy is sufficiently low, the interparticle interaction becomes important and starts compensating the focusing force of the wakefield. We know that this repelling force between two alongside-propagating electrons [Fig. 1(a)] scales inversely proportional to their energy $E = \gamma m_e c^2$, where γ is the Lorentz factor and m_e is the electron mass. If both particles propagate one behind the other [Fig. 1(b)] the interaction force scales like $1/E^2$. For this reason it is convenient to neglect any interparticle interaction between accelerated electrons in the bubble regime as long as the beam-load energy is in the GeV regime. For much lower energies between some tens of MeV and some hundreds of MeV and a transverse emittance of 10^{-9} m rad, alongside-propagating neighboring electrons will repel each other such that a spatial structure, which is known as the equilibrium structure of the beam load, can be considered. To analyze this structure a suitable description of the mutual electron interaction in the bubble is necessary.

One method to describe a retarded interaction of electrons within the bubble is to superpose the wakefield known from a quasistatic model with the interaction field described by the Liénard-Wiechert fields for relativistically moving pointlike
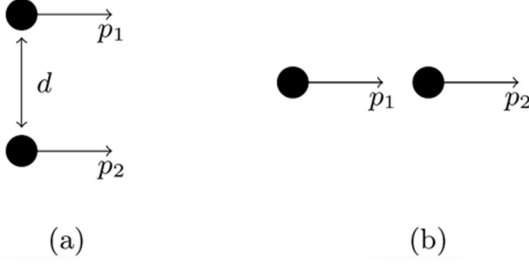
---

*lars.reichwein@hhu.de

FIG. 1. Schematic depiction of (a) two alongside-propagating particles and (b) two particles propagating one behind the other in the same direction.

charges. However, this approach would require knowledge of the history of all electrons within the beam load. To circumvent this disadvantage it is necessary to find an explicit expression of the retarded time in terms of the actual system time, the space variables, and the momentum variables. Once such an expression is found and substituted into the Liénard-Wiechert fields, a new quasistatic interaction model is derived. In this way the approximation of the retarded time effects the predicted equilibrium structure.

One important example for an interaction bubble model incorporating an explicit expression of the retarded time is introduced in Ref. [28] where two-dimensional (2D) and 3D equilibrium distributions are calculated on the basis of a Taylor expansion of the Liénard-Wiechert potentials in terms of v/c. Here, the series is cut after the second order because higher orders would require terms including the electron acceleration and thus radiation effects, too. Another argument given in Ref. [28] to cut the Taylor series after the second order is that retardation effects during the interaction of charged particles become small either if the particles move much slower than the speed of light or if the distance traveled by light in the time gap between the retarded time and actual time is large against the mean electron distance. In the scope of this approach it could be shown that the 2D equilibrium structure is similar to Wigner crystals observed in other areas of plasma physics, like dusty plasmas, while the 3D equilibrium distribution shows a completely new spatial symmetry.

In our current work we discuss an approach which allows us to calculate the retarded time with arbitrarily high precision and without knowledge of the electrons' history. We analyze the mutual electron interaction with a moderate energy up to some hundreds of MeV. At this energy level the interaction force between two alongside-propagating electrons is more than a hundred times stronger than it is for electrons traveling one behind the other. Thus we subdivide the beam load into multiple slices similar to the approach in Ref. [29] and discuss the results of this equilibrium slice model (ESM) for zero transverse emittance beam loads and full Liénard-Wiechert potentials. Afterward we compare our results to the 2D structure presented in Ref. [28] and discuss topological defects in the symmetry of the equilibrium distributions. We find that, while having a different size and more topological defects, similar hexagonal lattices as before are observed. The differences in size and number of defects can be explained by the more precise modeling of the system without Taylor expansions. An additional comparison of our numerical simulations to
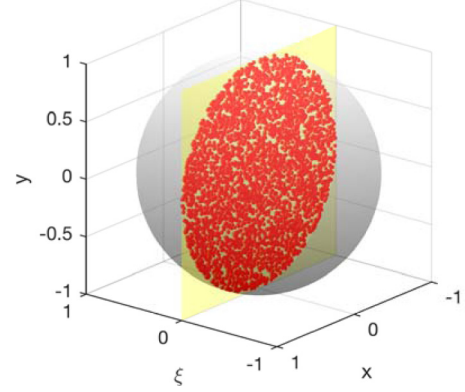

FIG. 2. Schematic depiction of the random distribution on a circular disk inside the bubble.

analytical scaling laws derived from a two-particle system of alongside-propagating relativistic electrons shows that the analytic scalings hold even for system with a much higher number of particles.

II. THE MATHEMATICAL MODEL

In the following we derive the Hamiltonian for a system of interacting alongside-accelerating relativistic electrons in external potentials in a moving coordinate system. In the scope of this model we analyze the equilibrium structure of electrons which are distributed on a circular disk inside a 3D bubble such that $\xi = z - V_0 t$ is the same for all electrons (Fig. 2, red dots on the yellow hyperplane). Here, z is the propagation direction of the bubble, V_0 is the bubble velocity, and ξ is the particles' longitudinal position inside the bubble in the moving system. The equilibrium structure is found by numerical simulations minimizing the Hamiltonian for the special case that the external potentials are known from the strongly simplified quasistatic 3D bubble model for electron acceleration in homogeneous plasma [8]. In this model the acceleration in the direction of propagation is just due to the external electric field $E_z = \partial \Psi / \partial \xi$, where $\Psi = \varphi - A_z = (x_i^2 + y_i^2 + \xi_i^2)/8$ is the wakefield potential.

The basic mathematical model for the electron-electron interaction is the retarded Liénard Wiechert potentials φ_{LW} and $\mathbf{A}_{\text{LW}}$, which originate from pointlike particles i with charge q_i, position $\mathbf{r}_i$, and velocity $\mathbf{v}_i$ at retarded time t_i and are measured at time t and position $\mathbf{r}$:

$$\varphi_{\text{LW}} = \sum_{i=1}^{n} \frac{q_i}{|\mathbf{r}(t) - \mathbf{r}_i(t_i)| - \frac{\mathbf{v}_i(t_i)}{c} \cdot [\mathbf{r}(t) - \mathbf{r}_i(t_i)]}, \quad (1)$$

$$\mathbf{A}_{\text{LW}} = \sum_{i=1}^{n} \frac{q_i \mathbf{v}_i(t_i)}{|\mathbf{r}(t) - \mathbf{r}_i(t_i)| - \frac{\mathbf{v}_i(t_i)}{c} \cdot [\mathbf{r}(t) - \mathbf{r}_i(t_i)]}. \quad (2)$$

From now on we normalize time to the inverse plasma frequency $\omega_p^{-1} = \sqrt{4\pi e^2 n_e / m_e}^{-1}$, lengths to the inverse plasma wave number $k_p^{-1} = c/\omega_p$, kinetic momenta to $m_e c$, energy to $m_e c^2$, fields to $m_e c \omega_p / e$, charges to the elementary charge e, masses to the electron rest mass m_e, and potentials to $m_e c^2 / e$.

To model the interparticle interaction by the Liénard-Wiechert potentials it is necessary to know the history of all

electrons within a slice or to find an explicit expression of the retarded time t_i in terms of the actual system time, the space variables, and the momentum variables. In the following we discuss the idea that all electrons in the slice are accelerated coherently such that they have the same (time-dependent) p_z and ξ but different constant radial positions r_i and thus $p_r = 0$. This approach is equivalent to the assumption that the electron ensemble is already in equilibrium and that we seek to find its spatial structure by minimizing the total energy of the system.

Since we assume that the kinetic energy of our electrons is much larger than their rest energy, $\gamma \gg \gamma_0$, and the solutions of the equations of motion of a single not-interacting test electron can be expressed in terms of the smallness parameter $\epsilon_0 = 1/(2\gamma_0^2)$. Written up to the second order in ϵ_0 the solutions are

$$p_z = p_0 - \frac{\xi_0}{2}(t - t_0) - \frac{\epsilon_0}{4}(t - t_0)^2, z = z_0 + \int_{t_0}^{t} \frac{p_z}{\gamma} dt'. \tag{3}$$

For boundary conditions $t_0 = 0$, $z(t_0) = \xi(t_0) = \xi_0$, and $p_z(t_0) = p_0$, our approximations result in implicit expressions for the positions and velocities of our electrons:

$$\mathbf{r}_i(t) = \begin{pmatrix} x_{i,0} \\ y_{i,0} \\ \xi_0 + \int_0^t v_z dt' \end{pmatrix}, \quad \mathbf{v}_i(t) = \frac{p_{iz}}{\gamma} \hat{e}_z. \tag{4}$$

In general, the retardation of time is given by $t_{\text{ret}} = t - |\mathbf{r}_i(t) - \mathbf{r}_j(t_{\text{ret}})|$, but for $t = t_0 = 0$ the retarded time of the jth particle simplifies to

$$\begin{aligned} t_j &= -|\mathbf{r}_i(t) - \mathbf{r}_j(t_j)| \\ &= -\sqrt{\Delta x_{ij}^2 + \Delta y_{ij}^2 + \left(\int_0^{t_j} v_z dt \right)^2}, \end{aligned} \tag{5}$$

where $\Delta x_{ij} = x_{i,0} - x_{j,0}$ and $\Delta y_{ij} = y_{i,0} - y_{j,0}$ describe the time-independent distance of particle i at time t to particle j at time t_j in the x or y direction, respectively.

Within this approach the particle positions are known analytically but the retarded times t_j still need to be computed numerically. The retarded Liénard Wiechert potentials, created by the jth particle and seen by the ith particle at time t, simplify to

$$\varphi_{ij} = \frac{\Lambda q_j \gamma_j}{-\gamma_j t_j + p_{zj} \int_0^{t_j} v_z dt}, \tag{6}$$

$$\mathbf{A}_{ij} = \frac{\Lambda q_j p_{zj}}{-\gamma_j t_j + p_{zj} \int_0^{t_j} v_z dt} \hat{e}_z. \tag{7}$$

Here, the prefactor $\Lambda = r_e / \lambda_{\text{pe}}$ consists of the classical electron radius $r_e = 2\pi e^2/(m_e c)^2$ and the plasma wavelength λ_{pe}. From now on we use the index j to indicate that we are using a variable that is given at the retarded time t_j and index i when dealing with the laboratory time $t = 0$. Then, the corresponding n-particle system Lagrangian is

$$\begin{aligned} L \approx \sum_{i=1}^{n} &\left[-\frac{1}{\gamma_i} + q_i \mathbf{v}_i \cdot \mathbf{A}(\mathbf{r}_i) - q_i \varphi(\mathbf{r}_i) \right] \\ &- \sum_{i>j} \left(1 - \frac{p_{iz} p_{jz}}{\gamma_i \gamma_j} \right) q_i \varphi_{ij} \end{aligned} \tag{8}$$

because all electrons move in one direction and have the same momentum. The first term in brackets is the Lagrangian of a free particle, while the second and third terms describe the coupling of the ith electron to the external potential. The last sum incorporates the retarded electron-electron interaction.

To calculate the Hamiltonian we need to know the canonical momentum π_i of each particle, which in principle is the strict derivative of the Lagrangian with respect to the velocity $\mathbf{v}_i$. Instead we, analogous to the calculation by Landau-Lifshitz [30], consider the term describing the interaction as perturbation. Then

$$\pi_i = \frac{\partial L}{\partial \mathbf{v}_i} \equiv \mathbf{p}_i + q_i \mathbf{A}(\mathbf{r}_i), \quad \mathbf{v}_i = \frac{\pi_i - q_i \mathbf{A}(\mathbf{r}_i)}{\gamma_i}, \tag{9}$$

and we only have to change the signs of the interaction parts. Furthermore, we perform a canonical transformation to the comoving frame, described by the coordinate ξ. Then

$$H = \sum_{i=1}^{n} \left[\gamma_i + q_i \Psi(\mathbf{r}_i) - p_{iz} + \sum_{i>j} \left(1 - \frac{p_{iz} p_{jz}}{\gamma_i \gamma_j} \right) q_i \varphi_{ij} \right]. \tag{10}$$

Since we will be using an iterative algorithm to find the energetic minimum of the system, we need the gradient of our Hamiltonian, which is given by

$$\begin{aligned} \nabla_{i\perp} H = \frac{1}{2} \begin{pmatrix} x_{i0} \\ y_{i0} \end{pmatrix} + \sum_{j \neq i} \left(1 - \frac{p_{iz} p_{jz}}{\gamma_i \gamma_j} \right) \nabla_{i\perp} \varphi_{ij} \\ - \sum_{j \neq i} \varphi_{ij} \left(\frac{p_{iz}}{\gamma_i} \frac{\partial}{\partial p_{jz}} \frac{p_{jz}}{\gamma_j} \frac{\partial p_{jz}}{\partial t_j} \nabla_{i\perp} t_j + \frac{p_{jz}}{\gamma_j} \nabla_{i\perp} \frac{p_{iz}}{\gamma_i} \right), \end{aligned} \tag{11}$$

where $\nabla_{i\perp} = \hat{e}_x \partial_{x_i} + \hat{e}_y \partial_{y_i}$. We cover the numerical procedure in further detail in Sec. IV, where we also present our numerical findings. In the next section we calculate the dependencies of the interparticle distance in equilibrium on our simulation parameters analytically, such that we can compare these to our simulation results.

III. SCALING LAWS

In the following we derive scaling laws for the mean interparticle distance Δr depending on the particles' energy and the plasma wavelength. To find an analytic expression, we consider the interaction of two equally charged alongside-propagating relativistic particles which experience two counteracting forces along their separation direction. The first force is the repelling interaction force $\mathbf{F}_\perp$ which can be calculated from the Liénard-Wiechert potentials. The second force is an external force $\mathbf{F}_{\text{ext}}$ which focused the particles to the origin but does not accelerate them in the direction of motion. Similar to the mathematical model we assume that the particles are resting in their equilibrium positions and calculate their distance. Due to the Colulomb interaction being a strictly two-particle effect in classical physics, we consider the interaction in the n-particle system as the sum of many two-particle interactions. In the following we conclude the scaling of the n-particle system from the two-particle case by separation of the contributions of the single parameters. This approach is rather heuristic but

holds for our simulations, as can be seen in the following section.

Starting from the scalar potential φ, we have

$$\varphi = \Lambda \frac{q_1 q_2}{|\mathbf{r}_1(t) - \mathbf{r}_2(t_2)| - \mathbf{v}_2(t_2) \cdot [\mathbf{r}_1 - \mathbf{r}_2(t_2)]}$$

$$= \Lambda \frac{q_1 q_2}{d_{12}} \cdot \frac{1}{1 - \mathbf{n}_2 \cdot \mathbf{v}_2(t_2)}, \qquad (12)$$

where

$$\mathbf{n}_2 = \frac{\mathbf{d}_{12}}{d_{12}}, \quad t_2 = -d_{12}, \quad d_{12} = |\mathbf{r}_1(t) - \mathbf{r}_2(t_2)|. \qquad (13)$$

Further, we have

$$\mathbf{F}_1 = -q_1 \nabla \varphi + q_1 \mathbf{v}_1 \times (\nabla \times \mathbf{A}),$$

$$\mathbf{v}_1 = v_1 \hat{\mathbf{e}}_z = v_2 \hat{\mathbf{e}}_z = \mathbf{v}_2 = \text{const.}, \qquad (14)$$

so that

$$\mathbf{F}_\perp = \mathbf{F}_1 = -\mathbf{F}_2 = -q_1 \left(1 - \mathbf{v}_1^2\right) \begin{pmatrix} \partial_x \\ \partial_y \\ 0 \end{pmatrix} \varphi_{12}, \qquad (15)$$

$$\mathbf{r}_2(t_2) = \mathbf{r}_2(t) - d_{12} \mathbf{v}_1. \qquad (16)$$

It is $\mathbf{r}_1(t) - \mathbf{r}_2(t) \perp \mathbf{v}_1$ so that the retarded time becomes

$$t_2 = -|\mathbf{r}_1(t) - \mathbf{r}_2(t)|\gamma = -d\gamma. \qquad (17)$$

We consider electrons with velocity $v_z \approx 1$, thus $v = |\mathbf{v}_1| = |\mathbf{v}_2| \approx 1$ and $q_1 = q_2 = -1$. Further, we assume that the electrons are located on the x axis. Then, with Eqs. (17) and (16) the interaction force is

$$F_x \approx -\frac{\Lambda}{\gamma^2} \frac{\partial}{\partial x} \frac{1}{d_{12} - [z_1 - z_2(t_2)]v}, \qquad (18)$$

where

$$d_{12} = |\mathbf{r}_1 - \mathbf{r}_2|\gamma = d\gamma, \quad d = x_1 - x_2. \qquad (19)$$

Since $z_1(t) = z_2(t)$, Eq. (16) gives

$$z_1 - z_2(t_2) = d\gamma v, \quad d_{12} - [z_1 - z_2(t_2)]v = \frac{d}{\gamma}, \qquad (20)$$

and thus

$$F_x = -\frac{\Lambda}{\gamma^2} \frac{\partial}{\partial x} \frac{\gamma}{d} = \frac{\Lambda}{\gamma} \frac{1}{d^2}. \qquad (21)$$

In equilibrium the magnitude of this force must be equal to the magnitude of the external force. In the bubble regime $|\mathbf{F}_{\text{ext}}| = r/2$, where $\Delta r = d = 2r$ due to the symmetry of the system such that

$$\Delta r = \sqrt[3]{\frac{4 r_e}{\lambda_{\text{pe}} \gamma}} \qquad (22)$$

in normalized units and

$$\Delta r = \sqrt[3]{\frac{r_e}{2\pi^3} \left(\frac{\lambda_{\text{pe}}}{\sqrt{\gamma}}\right)^{2/3}} \propto p^{-1/3} \lambda_{\text{pe}}^{2/3} \qquad (23)$$

in cgs units. This scaling holds for all systems of two alongside-propagating electrons with constant velocity and constant distance. In the mathematical model of the two-dimensional beam-load slice these conditions are fulfilled in part because we

assumed that all electrons have fixed radial positions and move with the same longitudinal velocity. This velocity, however, is not constant because we consider all particles to be accelerated coherently in the bubble in the longitudinal direction. Further, the physical system of the slice is an n-particle system but the interaction is modeled as a sum of two-particle interactions. Thus we expect that the scaling (23) holds for an arbitrary high but fixed number of electrons. The dependency on n in turn must be determined numerically and we do so in the following section. Moreover, we show that the idea of separating the single-parameter dependencies holds in our simulations.

Another important point regarding scaling laws is a comparison of our approach to the one presented in Ref. [28]. Here, a Taylor expansion of the Liénard-Wiechert potentials in terms of v/c was used to find the radially repelling interaction force

$$F_{\text{TR}} \propto \Lambda \frac{1}{\Delta r^2} \left(\frac{1}{\gamma} + \frac{v^2}{2}\right), \qquad (24)$$

while the external force $F_{\text{ext}} = r/2$ is the same as in our model. In the limit $v^2 \approx 1$ the equilibrium condition is

$$\Delta r_{\text{TR}}^3 \propto 2\Lambda \left(\frac{1}{\gamma} + \frac{1}{2}\right), \qquad (25)$$

so that

$$\Delta r_{\text{TR}} \propto \sqrt[3]{\frac{1}{\gamma} + \frac{1}{2}} \lambda_{\text{pe}}^{2/3} \qquad (26)$$

in cgs units. If we consider large electron energies $\gamma \gg 2$, the square root in Eq. (26) can be expanded in terms of γ^{-1} and the scaling of the mean electron distance in a 2D slice in the beam load becomes

$$\Delta r_{\text{TR}} \propto 2^{-2/3} \lambda_{\text{pe}}^{2/3} + \frac{2^{2/3}}{3} \lambda_{\text{pe}}^{2/3} \gamma^{-1}. \qquad (27)$$

If we compare Δr_{TR} to the scaling law in Eq. (23), we see that

$$\frac{\Delta r_{\text{TR}}}{\Delta r_{\text{LW}}} \propto \sqrt[3]{\frac{\gamma}{2}} + \frac{1}{3} \left(\frac{2}{\gamma}\right)^{2/3}. \qquad (28)$$

For high electron energies the second term approaches zero and

$$\frac{\Delta r_{\text{TR}}}{\Delta r_{\text{LW}}} \propto \sqrt[3]{\gamma}. \qquad (29)$$

This estimation clearly shows that the mean electron-equilibrium distances in the interaction model [28] are more than one order of magnitude larger than those predicted by our theory if the electrons have an energy in the near-GeV regime. For energies in the lower-MeV regime the difference between the distances predicted by the models is rather small and definitely in the same order.

IV. THE 2D EQUILIBRIUM STATE

In this section we present the numerical method we use to minimize the Hamiltonian in Eq. (10) and discuss the equilibrium structure in the 2D beam-load slices we find. In this context we compare the predictions of the scaling laws from the previous section to our numerical simulations for a fixed number of electrons and discuss topological defects.
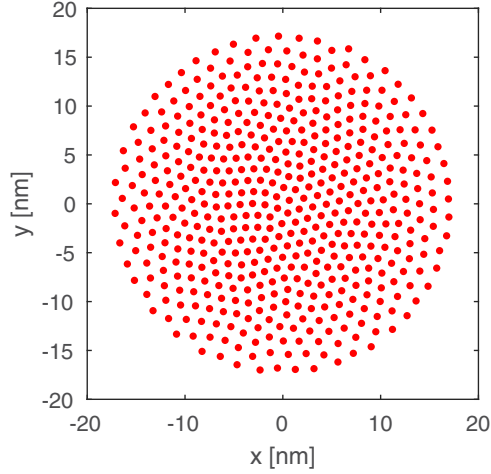
FIG. 3. Final distribution of a simulation with a momentum of $p = 125$ MeV/c and $n = 1000$ electrons with $\lambda_{pe} = 0.01$ cm.

Furthermore, the scaling of the mean particle distance in the equilibrium structure with the number of electrons is analyzed.

For our simulations we choose the steepest descent method to find the equilibrium structures. It is an iterative algorithm,

$$\mathbf{X}^{k+1} = \mathbf{X}^k - \nabla_k H \cdot \Delta t, \tag{30}$$

that shifts the particles' positions $\mathbf{X}^k = (\mathbf{r}_1^k, \ldots, \mathbf{r}_n^k)$ at time step k contrary to the direction of the gradient known from Eq. (11). The step size Δt is appropriately chosen in order to obtain the distribution $\mathbf{X}_0 = (x_{1,0}, y_{1,0}, \ldots, x_{n,0}, y_{n,0})$, such that $(\nabla_{\mathbf{X}} H)[\mathbf{X}_0]$ vanishes.

We distribute a fixed number of 100, 1000, or 4000 electrons randomly on a circular disk with a fixed ξ coordinate (see Fig. 2) inside the bubble and see hexagonal lattices as spatial equilibrium distribution (Fig. 3), analogous to Ref. [28].

In our simulations we vary the electron momenta between 25 and 500 MeV/c and observe a decrease in the mean particle distance Δr with increasing momentum which scales like

$$\Delta r_{phy} \propto p^{-1/3}, \tag{31}$$

as can be seen from the fit in Fig. 4. Here, Δr_{phy} is the average distance between the nearest neighbors in the lattice in cgs units given by a Delaunay triangulation [31]. Regarding the scaling of Δr in dependence of the plasma wavelength λ_{pe}, Fig. 5 shows that

$$\Delta r_{phy} \propto \lambda_{pe}^{2/3}. \tag{32}$$

These numerical scalings are in excellent agreement with our analytical approach in Eq. (23) in the section above. Furthermore, they coincide with the findings of Ref. [28], although our approach yields the correct prefactors.

For an increasing number of electrons we observe a decreasing trend for the mean distance between particles which scales like

$$\Delta r_{phy} \propto n^{-0.14}. \tag{33}$$

The corresponding fit in Fig. 6 shows an excellent correspondence.

Due to the confinement of the electrons in the harmonic bubble potential and their endeavor to repel each other, a

FIG. 5. Dependence of the mean particle distance for different plasma wavelengths. The simulations were done at 125 MeV/c for $n = 100$, 1000, and 4000 electrons.
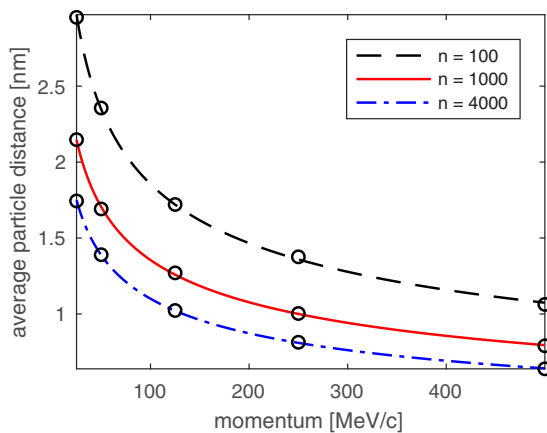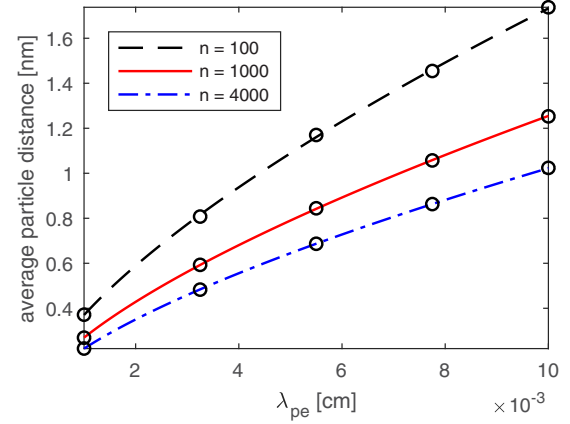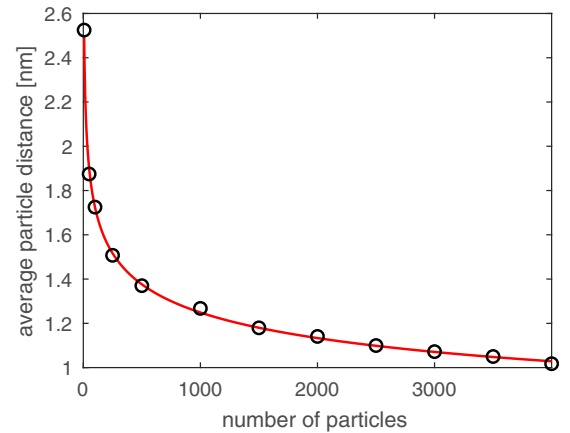

FIG. 4. Dependence of the mean particle distance for different momenta for $n = 100$, 1000, and 4000 electrons with $\lambda_{pe} = 0.01$ cm.

FIG. 6. Dependence of the mean particle distance for a different number of electrons and a constant momentum of 125 MeV/c with $\lambda_{pe} = 0.01$ cm.
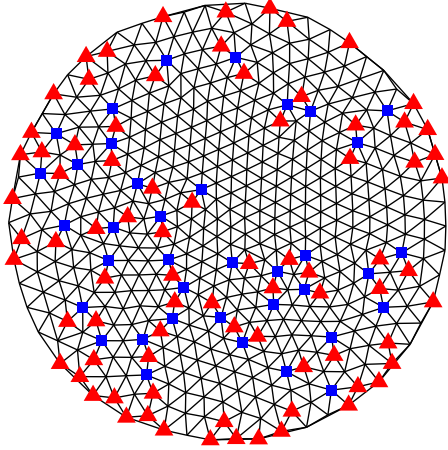
FIG. 7. Topological defects in a lattice consisting of 500 electrons. Marked as red triangles are electrons with a topological charge of -1, and marked as blue squares are particles with a topological charge of $+1$.
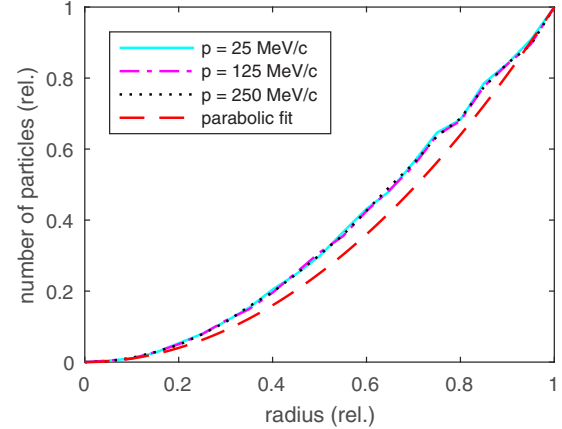

FIG. 8. Depiction of the number of electrons in dependence of the observed radius of the final distribution for different momenta. The dashed line depicts the reference curve of a constant surface density.

high amount of stress onto the lattice structure is produced. In order to reduce this stress, topological defects can arise. A topological defect is a deviation in the number of nearest neighbors from the reference value. We find these again with a Delaunay triangulation [31] such that we get the topological charge Q_{top} of each electron:

$$Q_{\text{top}} = \tilde{Q} - Q_{\text{nn}}. \qquad (34)$$

Here $\tilde{Q}$ is the reference value (in the case of our ideally hexagonal lattice $\tilde{Q} = 6$) and Q_{nn} is the actual number of nearest neighbors. A topological defect exists if $Q_{\text{top}} \neq 0$. Especially eye-catching is the formation of defect chains (alternating red triangles and blue squares in Fig. 7): electrons with only five nearest neighbors hold at least one neighbor that holds seven nearest neighbors of its own, etc. The increase of topological defects with increasing momentum is among other things explained by the higher stress put onto the lattice.

Regarding the density of our 2D distribution, we expect that the number of particles grows quadratically with the radius of the distribution for a constant density (Fig. 8). However, we can see that there is a higher electron density in the middle of the distribution, which declines towards the edge. This is mainly due to the fact that a transition between the hexagonal structure of the lattice and the circular symmetry of the confining potential is needed. Differences between the density gradients for different momenta or numbers of electrons, respectively, are negligible.

Different from Ref. [28], where mean interparticle distances in the range of $\Delta r_{\text{phy}} \approx 1$ nm were observed for $p = 270$ MeV/c and $n = 4000$ electrons at a plasma wavelength of $\lambda_{\text{pe}} = 11$ μm, our current approach predicts an average distance of $\Delta r_{\text{phy}} \approx 0.18$ nm. This is in good agreement with our analytic comparison in the previous section. For lower energies and larger plasma wavelengths, we observe interparticle distances in the nanometer range (Fig. 4), since on this scale electric and magnetic fields do not compensate

completely. Since we are able to calculate t_j with higher accuracy, we incorporate more of the retardation effects and therefore observe more deviations from a perfect hexagonal lattice than in Ref. [28]; i.e., more topological defects arise.

V. CONCLUSION

We have presented a method to find an explicit expression of the retarded time in terms of the actual system time, the space variables, and the momentum variables in order to avoid needing knowledge of the history of all electrons in a 2D beam-load slice. After substituting the retarded time into the Liénard-Wiechert potentials we introduced an ESM for relativistically moving pointlike test electrons as a superposition of the Liénard-Wiechert fields and the confining field from a quasistatic analytical bubble model. Since the model for the retarded time defines the interaction of the electrons, it also determines the equilibrium structure.

We derived scaling laws from a two-particle system of alongside-propagating relativistic electrons. These scalings fit perfectly to our numerical results even for a much higher number of particles. The equilibrium structure for many-particle systems is a hexagonal lattice, similar to the ones observed [28]. However, our approach yields smaller mean electron-electron distances. In the context of scaling laws we also showed that the difference between the distances predicted by models scales like $\sqrt[3]{\gamma}$. This is a moderate deviation for energies up to some hundreds of MeV. Finally, we discussed the existence of topological defects as a mean of reducing the stress onto the lattice, which is important for higher energies since a transition between the hexagonal lattice structure and the parabolic confinement of the external field needs to be made.

[1] I. Y. Kostyukov and A. Pukhov, Phys.-Usp. **58**, 81 (2015).

[2] T. Tajima and J. M. Dawson, Phys. Rev. Lett. **43**, 267 (1979).

[3] E. Esarey, C. Schroeder, and W. Leemans, Rev. Mod. Phys. **81**, 1229 (2009).

[4] A. Pukhov and J. Meyer-ter Vehn, Appl. Phys. B **74**, 355 (2002).

[5] O. Jansen, T. Tückmantel, and A. Pukhov, Eur. Phys. J.: Spec. Top. **223**, 1017 (2014).

[6] A. Pukhov and S. Gordienko, Philos. Trans. R. Soc., A **364**, 623 (2006).

[7] W. Lu, M. Tzoufras, C. Joshi, F. S. Tsung, W. B. Mori, J. Vieira, R. A. Fonseca, and L. O. Silva, Phys. Rev. Spec. Top.–Accel. Beams **10**, 061301 (2007).

[8] I. Kostyukov, A. Pukhov, and S. Kiselev, Phys. Plasmas **11**, 5256 (2004).

[9] P. Chen, J. M. Dawson, R. W. Huff, and T. Katsouleas, Phys. Rev. Lett **54**, 693 (1985).

[10] J. B. Rosenzweig, D. B. Cline, B. Cole, H. Figueroa, W. Gai, R. Konecny, J. Norem, P. Schoessow, and J. Simpson, Phys. Rev. Lett. **61**, 98 (1988).

[11] S. Huang, S. Y. Zhou, F. Li, Y. Wan, Y. P. Wu, J. F. Hua, C. H. Pai, W. Lu, Z. Wang, H. X. Deng, B. Liu, D. Wang, Z. T. Zhao, W. M. An, X. L. Xu, C. Joshi, and W. B. Mori, in *IPAC2017: Proceedings of the 8th International Particle Accelerator Conference, Copenhagen, Denmark, May 14–19, 2017* (Copenhagen, Denmark, 2017), p. 1734 .

[12] P. Baxevanis, M. J. Hogan, Z. Huang, M. Litos, B. O'Shea, T. O. Raubenheimer, J. C. Frisch, G. White, X. L. Xu, and W. Mori, AIP Conf. Proc. **1812**, 100013 (2017).

[13] J. Wang, J. Feng, C. Zhu, Y. Li, Y. He, D. Li, J. Tan, J. Ma, and L. Chen, Plasma Phys. Control. Fusion **60**, 034004 (2018).

[14] A. Gonsalves, B. Pollock, and W. Lu, AIP Conf. Proc. **1812**, 030001 (2017).

[15] A. Martinez de la Ossa, Z. Hu, M. J. V. Streeter, T. J. Mehrling, O. Kononenko, B. Sheeran, and J. Osterhoff, Phys. Rev. Accel. Beams **20**, 091301 (2017).

[16] M. P. Tooley, B. Ersfeld, S. R. Yoffe, A. Noble, E. Brunetti, Z. M. Sheng, M. R. Islam, and D. A. Jaroszynski, Phys. Rev. Lett **119**, 044801 (2017).

[17] A. J. Gonsalves, K. Nakamura, C. Lin, D. Panasenko, S. Shiraishi, T. Sokollik, C. Benedett, C. B. Schroeder, C. G. R. Geddes, J. van Tilborg, J. Osterhoff, E. Esarey, C. Toth, and W. P. Leemans, Nat. Phys. **7**, 862 (2011).

[18] K. K. Swanson, H.-E. Tsai, S. K. Barber, R. Lehe, H.-S. Mao, S. Steinke, J. van Tilborg, K. Nakamura, C. G. R. Geddes, C. B. Schroeder, E. Esarey, and W. P. Leemans, Phys. Rev. Accel. Beams **20**, 051301 (2017).

[19] X. L. Xu, F. Li, W. An, T. N. Dalichaouch, P. Yu, W. Lu, C. Joshi, and W. B. Mori, Phys. Rev. Accel. Beams **20**, 111303 (2017).

[20] J. Xu, A. Buck, S.-W. Chou, K. Schmid, B. Shen, T. Tajima, M. C. Kaluza, and L. Veisz, Phys. Plasma **24**, 083106 (2017).

[21] A. Pak, K. A. Marsh, S. F. Martins, W. Lu, W. B. Mori, and C. Joshi, Phys. Rev. Lett. **104**, 025003 (2010).

[22] S. Tochitsky, F. Fiuza, and C. Joshi, AIP Conf. Proc. **1777**, 020005 (2016).

[23] B. Hidding, G. Pretzler, J. B. Rosenzweig, T. Königstein, D. Schiller, and D. L. Bruhwiler, Phys. Rev. Lett. **108**, 035001 (2012).

[24] B. Hidding, J. B. Rosenzweig, Y. Xi, B. O'Shea, G. Andonian, D. Schiller, S. Barber, O. Williams, G. Pretzler, T. Königstein, F. Kleeschulte, M. J. Hogan, M. Litos, S. Corde, W. W. White, P. Muggli, D. L. Bruhwiler, and K. Lotov, AIP Conf. Proc. **1507**, 570 (2012).

[25] M. Chen, E. Esarey, C. G. R. Geddes, E. Cormier-Michel, C. B. Schroeder, S. S. Bulanov, C. Benedetti, L. L. Yu, S. Rykovanov, D. L. Bruhwiler, and W. P. Leemans, Phys. Rev. Spec. Top.–Accel. Beams **17**, 051303 (2014).

[26] M. Schnell, A. Sävert, B. Landgraf, M. Reuter, M. Nicolai, O. Jäckel, C. Peth, T. Thiele, O. Jansen, A. Pukhov, O. Willi, M. C. Kaluza, and C. Spielmann, Phys. Rev. Lett. **108**, 075001 (2012).

[27] A. Sävert, S. P. D. Mangles, M. Schnell, E. Siminos, J. M. Cole, M. Leier, M. Reuter, M. B. Schwab, M. Möller, K. Poder, O. Jäckel, G. G. Paulus, C. Spielmann, S. Skupin, Z. Najmudin, and M. C. Kaluza, Phys. Rev. Lett **115**, 055002 (2015).

[28] J. Thomas, M. M. Günther, and A. Pukhov, Phys. Plasmas **24**, 013101 (2017).

[29] D. Schulte, CERN Yellow Rep.: School Proc. **3**, 431 (2017).

[30] L. Landau and E. Lifschitz, *Lehrbuch der Theoretischen Physik II: Klassische Feldtheorie*, (Harri Deutsch, Frankfurt am Main, 2009), p. 496.

[31] A. Radzvilavičius and E. Anisimovas, J. Phys.: Condens. Matter **23**, 385301 (2011).